Classical mechanics of two-electron atoms

Klaus Richter
Division de Physique Théorique, Institut de Physique Nucléaire, 91406 Orsay, France

Gregor Tanner and Dieter Wintgen
Fakultät für Physik, Universität Freiburg, Hermann-Herder-Strasse 3, 79104 Freiburg, Germany
(Received 7 June 1993)

We study the classical electron motion of two-electron atoms. We present techniques to regularize singularities in the equations of motion and to calculate stability properties of periodic orbits in six-dimensional phase space. Depending on the configuration of the electron pair, the classical phase space turns out to be regular, purely chaotic, or of mixed structure. For the fully hyperbolic case of collinear electron motion, a strong correlation between ionizing trajectories and the collision manifold of the triple collision is found. For the near-integrable collinear motion with both electrons on the same side of the atom we (numerically) derive an action-angle representation of the Hamiltonian.

PACS number(s): 31.20.Tz, 03.20.+i, 05.45.+b

I. INTRODUCTION

The three-body problem of celestial mechanics is one of the most famous problems of theoretical physics. A huge number of papers has been published which deals with the nonintegrable classical motion of three bodies under the influence of their mutual gravitational interactions [1]. In contrast, only a limited number of papers deals with the classical mechanics of the (microscopic) three-body Coulomb (TBC) problem. Particularly, a systematic analysis of the classical phase space of two-electron atoms, such as the helium atom as the prototype system of the atomic TBC problem, is non-existent. Quantitative classical studies are complicated by the multidimensionality, the nonseparability, and the unbound character of the motion which is governed by singular and long-ranged potentials.

Investigations of two-electron atoms usually focus on the quantum aspects of the system in terms of approximate solutions of the corresponding Schrödinger equation. However, the development of techniques to excite and spectroscopy highly-doubly-excited states of two-electron atoms [2–5] allows one to study electron dynamics and correlations in a semiclassical energy regime where the excited electron pair carries features of classical moving particles. Thus highly-doubly-excited atoms are sometimes referred to as *planetary atoms* [6] due to their similarity to the gravitational three-body problem. However, a direct transfer of results from the celestial to the atomic three-body problem is not possible for two reasons.

(i) In gravitational three-body systems the masses of the bodies involved usually differ by orders of magnitude. Since the gravitational interaction depends on the particle masses, perturbative treatments are sufficient in many cases. On the contrary, the Coulomb interactions in two-electron atoms such as helium are of the same order of magnitude and therefore do not allow *ad hoc* a perturbative treatment. In addition, due to the high degeneracy of the independent-particle limit $1/Z = 0$ (Z is the nuclear charge) an application of the Kol'mogorov-Arnol'd-Moser (KAM) theory to derive an independent-particle limit is impossible.

(ii) Gravitational forces are always attractive. In the TBC problem, however, one interparticle interaction is repulsive, which often leads to a destabilization of the system. Depending on the initial conditions the classical two-electron atom usually autoionizes after a few revolutions of the electrons around the nucleus.

A systematic investigation of the classical properties of two-electron atoms is also desirable because it provides the necessary classical information for modern semiclassical methods which have become powerful tools for the study of excited states in atomic and molecular systems [7–9]. The semiclassical techniques for nonseparable systems are usually based on the periodic-orbit (PO) theory of Gutzwiller [10] which allows one to approximate the quantum level density in terms of classical periodic orbits. Recently several authors [9,11–18] applied PO theory to obtain semiclassical resonance energies for two-electron atoms.

In this paper we will report on our investigation of the classical phase-space structure of two-electron atoms with an emphasis on helium. The paper is organized as follows. In Sec. II we will give a general characterization of the problem. In Sec. III we introduce a transformation to regularize Coulomb potential singularities, which is an essential ingredient for a proper classical treatment. We describe methods to solve the classical equations of motion and to calculate stability exponents for periodic orbits in three dimensions using local coordinates for the orbits. For total angular momentum $L = 0$ there are three symmetry planes where the motion reduces essentially to two degrees of freedom, the third degree of freedom being in a static equilibrium. If we describe the electron pair in terms of their radial distances r_1, r_2 from the nucleus and the angle Θ between their radius vectors the symmetry planes are characterized by (i) $r_1 = r_2$, (ii) $\Theta = \pi$, and (iii) $\Theta = 0$. In Secs. IV–VI we study con-

figurations where the electrons are grouped near these symmetry planes. The classical phase space turns out to be of mixed regular-chaotic (i), chaotic (ii), and near-integrable (iii) structure.

II. CHARACTERIZATION OF THE PROBLEM

A. Constants of motion

A three-body system can be described in terms of nine (Cartesian) coordinates but there exist ten independent constants of motion which allow one to reduce the degrees of freedom [19]. Six integrals of motion describe the uniform center of mass motion $\mathbf{r}_{\mathrm{c.m.}}(t) = \mathbf{v}_0 t + \mathbf{r}_0$. The transformation to the center of mass system reduces the phase space from 18 to 12 dimensions. The three components of the conserved total angular momentum $\mathbf{L}$ allow for a further reduction to nine phase-space dimensions. Since the system is invariant with respect to rotations around $\mathbf{L}$ (the conjugated angle can be chosen arbitrarily) we can diminish the number of coordinates again by one (elimination of the knots [19]). Therefore we end up with a conservative system with four degrees of freedom and eight-dimensional phase space (the total energy E is an additional constant of motion).

In the present paper we focus on three-body configurations with $L = 0$. Then the motion of the particles is confined to a plane fixed in configuration space [19] and reduces to three degrees of freedom. We take the interparticle distances as dynamical variables.

B. Hamiltonian and scaling property

The Hamiltonian for three particles with charges Z_i and masses m_i moving in a plane (x, y) reads

$$\mathcal{H} = \sum_{i=1}^{3} \frac{\mathbf{p}_i^2}{2m_i} + \frac{Z_1 Z_2}{r_{12}} + \frac{Z_1 Z_3}{r_{13}} + \frac{Z_2 Z_3}{r_{23}} \,. \tag{1}$$

r_{ij} are the interparticle distances

$$r_{ij} = [\,(x_i - x_j)^2 + (y_i - y_j)^2]^{\frac{1}{2}} \,. \tag{2}$$

The Hamiltonian (1) is homogeneous in coordinates and momenta. Thus by introducing energy scaled quantities

$$\begin{aligned} r^{\mathrm{sc}} &= |E| r, \\ p^{\mathrm{sc}} &= |E|^{-\frac{1}{2}} p, \\ t^{\mathrm{sc}} &= |E|^{\frac{3}{2}} t, \end{aligned} \tag{3}$$

the Hamiltonian can be transformed to energy independent form

$$\begin{aligned} \mathcal{H}^{\mathrm{sc}} &= \sum_{i=1}^{3} \frac{\mathbf{p}_i^{\mathrm{sc}\,2}}{2m_i} + \frac{Z_1 Z_2}{r_{12}^{\mathrm{sc}}} + \frac{Z_1 Z_3}{r_{13}^{\mathrm{sc}}} + \frac{Z_2 Z_3}{r_{23}^{\mathrm{sc}}} \\ &= E^{\mathrm{sc}} = \begin{cases} +1, & E > 0 \\ 0, & E = 0 \\ -1, & E < 0 \end{cases} \,. \end{aligned} \tag{4}$$

$E = 0$ denotes the three-particle breakup threshold. The energy regime below this threshold for double ionization is (uniformly) characterized by $E^{\mathrm{sc}} = -1$: The classical phase space depends on the particle masses and charges only. Nearly all electron configurations are energetically allowed to autoionize classically. Only the quantization of classical motion prevents an exchange of arbitrary amounts of energy between the electrons and leads to the existence of bound (quantum) states. In the following we focus on negative energies which cover the regime of possible resonance formation in the system. For positive energies every trajectory represents a doubly ionized system.

The scaling property (3) yields the relation $L^{\mathrm{sc}} = \sqrt{|E|} L$ between the scaled angular momentum (L^{sc}) and the physical angular momentum L. Keeping L fixed, L^{sc} converges to zero with increasing electronic excitation ($E \to 0$). This means that the dynamics of *highly* doubly-excited states with moderate angular momentum $L \neq 0$ (e.g., atomic P, D, F states) can be approximated by the planar configuration $L^{\mathrm{sc}} = 0$.

C. Symmetries of two-electron atoms

For a two-electron atom (if not stated otherwise, we use atomic units, i.e., $m_1 = m_2 = 1$, $Z_1 = Z_2 = -1$, and the simplified notation $\mathbf{r}_{13} = \mathbf{r}_1, \mathbf{r}_{23} = \mathbf{r}_2$) the Hamiltonian (4) is invariant with respect to reflection $(\mathbf{r}_1, \mathbf{r}_2) \to (-\mathbf{r}_1, -\mathbf{r}_2)$ and particle exchange $(\mathbf{r}_1, \mathbf{r}_2) \to (\mathbf{r}_2, \mathbf{r}_1)$. Classical dynamics does not account for the Pauli principle. However, the particle exchange symmetry of the Hamiltonian reduces the accessible configuration space to the fundamental domain [9], i.e., the fully desymmetrized region of configuration space with $r_1 > r_2$.

For $L = 0$ special two-dimensional symmetry planes exist which are characterized by the property that electron-pair motion which initially lies in one of the planes will remain there for all times. The three-dimensional motion essentially reduces to two degrees of freedom. The three existing invariant subspaces are (Θ denotes the angle between $\mathbf{r}_1$ and $\mathbf{r}_2$) (i) the *Wannier saddle* (see Sec. IV) $r_1 \equiv r_2$; $p_{r_1} \equiv p_{r_2}$, (ii) the $e^- Z e^-$ configuration (see Sec. V) $\Theta \equiv \pi$; $p_\Theta \equiv 0$, (iii) the $Z e^- e^-$ configuration (see Sec. VI) $\Theta \equiv 0$; $p_\Theta \equiv 0$.

III. METHODS OF SOLVING THE EQUATIONS OF MOTION

A. Regularization

Whenever an interparticle distance vanishes (particle collision) the potential energy diverges. Thus, an essential requirement of the classical analysis is the regularization of the motion. There is a striking difference in the topology of possible collisions. In analogy to the two-body Coulomb problem the motion can be regularized for binary collisions, where only one interparticle distance vanishes. In contrast, the triple collision ($r_1 = r_2 = r_{12} = 0$) cannot be regularized, i.e., the corresponding solutions have branch points of infinite order [20].

The regularization of the two-particle Coulomb prob-

lem has been performed by Kustaanheimo and Stiefel (KS) by transforming the Coulomb problem to a system of two two-dimensional harmonic oscillators [21]. In the following we follow a work of Aarseth and Zare [22] from celestial mechanics which is based on a simultaneous application of two KS transformations to regularize two binary collisions of the three-body problem.

In a first step we transform the planar system given by the Hamiltonian (4) to the center of mass system [dropping the indices (sc)]:

$$\begin{aligned} &\mathbf{r}_1' = \mathbf{r}_1 - \mathbf{r}_3 \quad , \quad \mathbf{r}_2' = \mathbf{r}_2 - \mathbf{r}_3 \quad , \quad \mathbf{r}_3' = \mathbf{r}_3 \, , \\ &\mathbf{p}_1' = \mathbf{p}_1 - \mathbf{p}_{\text{c.m.}} \; ; \quad \mathbf{p}_2' = \mathbf{p}_2 - \mathbf{p}_{\text{c.m.}} \; ; \\ &\mathbf{p}_3' = \mathbf{p}_1 + \mathbf{p}_2 + \mathbf{p}_3 = \mathbf{p}_{\text{c.m.}} \equiv \mathbf{0} \, . \end{aligned} \tag{5}$$

The transformed Hamiltonian is reduced from six to four degrees of freedom and reads ($E = -1$)

$$\mathcal{H}' = -1 = \frac{1}{2\mu_{13}}\mathbf{p}_1'^2 + \frac{1}{2\mu_{23}}\mathbf{p}_2'^2 + \frac{1}{m_3}\mathbf{p}_1' \cdot \mathbf{p}_2' + \frac{Z_1 Z_3}{r_1'} + \frac{Z_2 Z_3}{r_2'} + \frac{Z_1 Z_2}{r_{12}'} \, . \tag{6}$$

$\mu_{k3} = m_k m_3/(m_k + m_3)$ are the reduced masses and

$$\begin{aligned} r_i' &= [\, x_i'^2 + y_i'^2 \,]^{\frac{1}{2}} \qquad (i = 1, 2), \\ r_{12}' &= [\, (x_1' - x_2')^2 + (y_1' - y_2')^2 \,]^{\frac{1}{2}} \end{aligned} \tag{7}$$

are the interparticle distances. For the following regularization it is convenient to keep four coordinates although a reduction to three coordinates would be possible by employing the relation $L = 0$.

We introduce regularized coordinates

$$\begin{aligned} &\mathbf{R}_1 = (Q_1, Q_2) \quad , \quad \mathbf{R}_2 = (Q_3, Q_4), \\ &\mathbf{P}_1 = (P_1, P_2) \quad , \quad \mathbf{P}_2 = (P_3, P_4) \, , \end{aligned} \tag{8}$$

which are defined by means of the transformations (omitting the primes of the coordinates x, y, r)

$$\begin{aligned} &x_1 = Q_1^2 - Q_2^2, \quad y_1 = 2\,Q_1\,Q_2, \quad r_1 = R_1^2 = Q_1^2 + Q_2^2 \, , \\ &x_2 = Q_3^2 - Q_4^2, \quad y_2 = 2\,Q_3\,Q_4, \quad r_2 = R_2^2 = Q_3^2 + Q_4^2 \, , \end{aligned} \tag{9}$$

$$\begin{aligned} p_{x_1} &= \frac{Q_1 P_1 - Q_2 P_2}{2R_1^2}, \quad p_{y_1} = \frac{Q_2 P_1 + Q_1 P_2}{2R_1^2} \, ; \\ p_{x_2} &= \frac{Q_3 P_3 - Q_4 P_4}{2R_2^2}, \quad p_{y_2} = \frac{Q_4 P_3 + Q_3 P_4}{2R_2^2} \, . \end{aligned}$$

In addition, a fictive time τ,

$$dt = r_1\, r_2\, d\tau \, , \tag{10}$$

is introduced. Thereby, velocities dx/dt diverging at the Coulomb singularities are replaced by smoothed velocities $dx/d\tau$.

The regularized Hamiltonian finally reads

$$H = 0 = \frac{1}{8\mu_{13}} R_2^2\, \mathbf{P}_1^2 + \frac{1}{8\mu_{23}} R_1^2\, \mathbf{P}_2^2 + \frac{1}{4m_3}[(\mathbf{R}_1 \cdot \mathbf{R}_2)(\mathbf{P}_1 \cdot \mathbf{P}_2) - (\mathbf{P}_1 \times \mathbf{P}_2) \cdot (\mathbf{R}_1 \times \mathbf{R}_2)] + Z_1\, Z_3\, R_2^2 + Z_2\, Z_3\, R_1^2 + R_1^2\, R_2^2 \left(1 + \frac{Z_1\, Z_2}{R_{12}^2}\right) , \tag{11}$$

with

$$R_{12}^2 = r_{12} = [(Q_1^2 + Q_2^2)^2 + (Q_3^2 + Q_4^2)^2 - 2(Q_1 Q_3 + Q_2 Q_4)^2 + 2(Q_1 Q_4 - Q_2 Q_3)^2]^{\frac{1}{2}} \tag{12}$$

and with τ as the new time variable.

The derivation of (11) by means of canonical transformations can be found in Ref. [22]. The regularization technique can be extended to $L \neq 0$ with four independent degrees of freedom. The Hamiltonian (11) exhibits a form similar to two two-dimensional coupled harmonic oscillators with modified kinetic energy.

We study the classical motion by numerically solving Hamilton's equations of motion

$$\frac{dQ_i}{d\tau} = \frac{dH}{dP_i} \quad , \quad \frac{dP_i}{d\tau} = -\frac{dH}{dQ_i} \, . \tag{13}$$

For a TBC system we conveniently choose $Z_1 Z_2/r_{12}$ as the repulsive potential as the binary collision $r_{12} = R_{12}^2 = 0$ is forbidden by energy conservation for nonvanishing r_1, r_2. The equations of motion become singular only in the case of the triple collision ($r_1 = r_2 = r_{12} = 0$). Nevertheless, since R_1, R_2 approach zero for $R_{12} \to 0$ the form of the singular potential $Z_1\, Z_2\, R_1^2\, R_2^2/R_{12}^2$ in Eq. (11) allows for a stable and fast numerical integration of trajectories passing nearby the triple collision.

B. Periodic orbits

Periodic orbits of chaotic systems lie close in phase space. Therefore they may serve as representatives to describe the classical phase-space flow [23]. The behavior of nearby (nonperiodic) trajectories can be approximated by means of the stability indices of the PO. The idea to characterize the classical dynamics by local properties of PO (action, period, stability, topological indices) has also been employed in the semiclassical PO theory of nonintegrable systems [10] uncovering their key role in the description of general dynamical properties. We now summarize our techniques to calculate the relevant classical quantities.

1. Action and period

The (scaled) action along a PO with period T^{sc} is given by

$$S^{\text{sc}} = \oint_{\text{PO}} (\mathbf{P}_1 \cdot d\mathbf{R}_1 + \mathbf{P}_2 \cdot d\mathbf{R}_2) \tag{14}$$

$$= \int_0^{T^{sc}} \left(\mathbf{P}_1 \cdot \frac{\partial H}{\partial \mathbf{R}_1} + \mathbf{P}_2 \cdot \frac{\partial H}{\partial \mathbf{R}_2} \right) d\tau \,. \tag{15}$$

Due to the scaling property of the Hamiltonian (11) we derive from the general expression

$$T = \frac{\partial S}{\partial E} \tag{16}$$

the simple relation

$$T^{sc} = (-E)^{\frac{3}{2}} T = (-E)^{\frac{3}{2}} \frac{\partial}{\partial E} (-E)^{-\frac{1}{2}} S^{sc} = \frac{1}{2} S^{sc} \tag{17}$$

between the scaled action and the period of a PO in the TBC system.

2. Stability indices

The stability of a PO can be calculated by making use of the symplectic structure of the equations of motion [24, 25]. The TBC system is described by means of the vector

$$\gamma = (Q_1, Q_2, Q_3, Q_4, P_1, P_2, P_3, P_4) \tag{18}$$

in the eight-dimensional phase space. With the help of the symplectic unit matrix

$$\mathbf{J} = \begin{pmatrix} \mathbf{0} & \mathbf{1} \\ -\mathbf{1} & \mathbf{0} \end{pmatrix} , \tag{19}$$

which is composed of 4×4 matrices $\mathbf{0}$ and $\mathbf{1}$, Hamilton's equations of motion can be brought to the compact form

$$\frac{d\gamma}{d\tau} = \mathbf{J} \left(\frac{\partial H}{\partial \gamma} \right) . \tag{20}$$

We will study the behavior of classical paths in the vicinity of a PO $\gamma_{PO}(\tau)$. After one period a trajectory with initial condition $\gamma(0) = \gamma_{PO} + \delta\gamma(0)$ will reach the point $\gamma(T) = \gamma_{PO} + \delta\gamma(T)$ in phase space. We obtain the linear relation

$$\delta\gamma(T) = \mathbf{M}[\gamma_{PO}; T]\, \delta\gamma(0) \tag{21}$$

between an infinitesimal initial deviation $\delta\gamma(0)$ and the final deviation $\delta\gamma(T)$. In Eq. (21) $\mathbf{M}$ is the so-called monodromy matrix with elements defined as

$$M_{ij}[\gamma_{PO}; \tau] := \frac{\partial \gamma_i(\tau)}{\partial \gamma_j(0)} \tag{22}$$

and represents the linear approximation of the flux around the PO. From Eqs. (20) and (22) we obtain the equations of motion for $\mathbf{M}$,

$$\frac{d\mathbf{M}}{d\tau} = \mathbf{J} \left. \frac{\partial^2 H}{\partial \gamma^2} \right|_{\gamma_{PO}} \mathbf{M} \quad , \qquad \mathbf{M}(0) \equiv \mathbf{1}, \tag{23}$$

which allows one to integrate $\mathbf{M}$ along a PO.

The stability of a PO is given by means of the eigenvalues Λ of $\mathbf{M}(T)$ which come in pairs or quadruplets. (If Λ is an eigenvalue of $\mathbf{M}$ so are $1/\Lambda$, Λ^*, and $1/\Lambda^*$.) They can be classified as follows [10].

(i) elliptical, if $\Lambda = \exp(\pm 2\pi i\nu)$ with ν being real. The winding number ν describes the stable revolution of adjacent trajectories around a PO.

(ii) (inverse) marginally stable if $\Lambda = +1$ ($\Lambda = -1$).

(iii) (inverse) hyperbolic if $\Lambda = \exp(\pm\lambda)$ [$\Lambda = -\exp(\pm\lambda)$] where $\lambda > 0$ (real) is the stability exponent, sometimes called the Lyapunov exponent of the PO.

(iv) Loxodromic if $\Lambda = \exp(\pm u \pm i\psi)$, with u, ψ being real numbers.

The loxodromic case is peculiar for motion with more than two degrees of freedom. We numerically obtain winding numbers and Lyapunov exponents by integration of $\mathbf{M}$ according to Eq. (23).

3. Monodromy matrix in local coordinates

The (8×8)-monodromy matrix has four pairs of eigenvalues whose products are equal to unity. Due to the conservation of energy E and angular momentum

$$\begin{aligned} L &= x_1 p_{y_1} - y_1 p_{x1} + x_2 p_{y_2} - y_2 p_{x2} \\ &= \tfrac{1}{2}(Q_1 P_2 - P_1 Q_2 + Q_3 P_4 - P_3 Q_4) \end{aligned} \tag{24}$$

four of these eigenvalues are trivial and equal to one, the corresponding eigenvectors can be constructed explicitly.

The overall motion is confined to the six-dimensional subspace of the energy and angular-momentum shell. Thus a deviation in energy, $\delta E = \delta\gamma(\tau) \cdot \nabla H(\tau)$ with $\nabla H = \left(\frac{\partial H}{\partial \mathbf{Q}}, \frac{\partial H}{\partial \mathbf{P}} \right)_{\gamma(\tau)}$, is conserved along every trajectory $\gamma(\tau)$. The vector

$$\gamma_E = \frac{\nabla H}{|\nabla H|^2} \tag{25}$$

measures the projection of $\delta\gamma$ perpendicular to the energy shell in units of δE. It is an eigenvector of $\mathbf{M}$ with eigenvalue one after one period of a PO. By analogy, the vector

$$\begin{aligned} \gamma_L &= \frac{\nabla L}{|\nabla L|^2} \\ &= 2 \frac{(P_2, -P_1, P_4, -P_3, -Q_2, Q_1, -Q_4, Q_3)^T}{Q_1^2 + Q_2^2 + Q_3^2 + Q_4^2 + P_1^2 + P_2^2 + P_3^2 + P_4^2} \end{aligned} \tag{26}$$

measures deviations perpendicular to the angular-momentum shell in units of the conserved quantity δL.

An initial displacement $\delta\tau$ in time remains constant along a trajectory $\gamma(\tau)$ and is directed along the phase-space velocity

$$\gamma_T = \frac{d\gamma}{d\tau} = (\dot{\mathbf{Q}}, \dot{\mathbf{P}}) = \left(\frac{\partial H}{\partial \mathbf{P}}, -\frac{\partial H}{\partial \mathbf{Q}} \right) = \mathbf{J} \nabla H \,. \tag{27}$$

Correspondingly, an initial displacement in the angle ϕ in the plane perpendicular to the angular-momentum vector $\mathbf{L}$ is conserved along a trajectory. The associated phase-space vector is given by

$$\begin{aligned} \gamma_\phi &= \frac{\partial \gamma}{\partial \phi} = \{\gamma, L\} \\ &= (-Q_2, Q_1, -Q_4, Q_3, -P_2, P_1, -P_4, P_3)^T = \mathbf{J} \nabla L, \end{aligned} \tag{28}$$

where $\{\,\}$ are the Poisson brackets. We can separate these four trivial directions from those describing the nontrivial motion around a trajectory by a transformation to a local coordinate system. The local system is constructed from the four linear independent vectors $\gamma_E, \gamma_T, \gamma_L$, and γ_ϕ and a local orthogonal Vierbein which in general has to be determined numerically. However, an analytical construction of a complete orthogonal local basis set is possible [26], if the motion takes place in one of the symmetry planes.

We will denote the basis vectors of the Vierbein which lie perpendicular to the trajectory but within a symmetry plane by $\gamma_i^{\parallel}$ $(i = 1,2)$, and those which are directed orthogonal to the symmetry plane by $\gamma_i^{\perp}$ $(i = 1,2)$. The local orthogonal basis is thus given by the set $\{\gamma_1^{\parallel}, \gamma_2^{\parallel}, \gamma_1^{\perp}, \gamma_2^{\perp}, \gamma_E, \gamma_T, \gamma_L, \gamma_\phi\}$. The matrix

$$\mathbf{O} = (\gamma_1^{\parallel}, \gamma_2^{\parallel}, \gamma_1^{\perp}, \gamma_2^{\perp}, \gamma_E, \gamma_T, \gamma_L, \gamma_\phi) \tag{29}$$

generates a transformation between the global variables $\mathbf{Q}, \mathbf{P}$ and a local basis system of the trajectory. The monodromy matrix $\mathbf{m}(\tau)$

$$\mathbf{m}(\tau) = \mathbf{O}^{-1}(\tau)\, \mathbf{M}(\tau)\, \mathbf{O}(0) \tag{30}$$

describes the linearized motion along a trajectory in the local coordinates and the differential equation (23) transforms to [25]

$$\frac{d\mathbf{m}}{d\tau} = \boldsymbol{l}|_{\gamma_{\rm PO}}\, \mathbf{m},$$

with

$$\boldsymbol{l} = \mathbf{O}^{-1} \left(\mathbf{J}\, \frac{\partial^2 H}{\partial \gamma^2} \mathbf{O} - \frac{d\mathbf{O}}{d\tau} \right). \tag{31}$$

In this basis set the local monodromy matrix $\mathbf{m}$ has the form

$$\begin{pmatrix} \delta\gamma_1^{\parallel} \\ \delta\gamma_2^{\parallel} \\ \delta\gamma_1^{\perp} \\ \delta\gamma_2^{\perp} \\ \delta E \\ \delta\tau \\ \delta L \\ \delta\phi \end{pmatrix} (\tau) = \begin{pmatrix} m_{11}^{\parallel} & m_{12}^{\parallel} & c_{13} & c_{14} & * & 0 & * & 0 \\ m_{21}^{\parallel} & m_{22}^{\parallel} & c_{23} & c_{24} & * & 0 & * & 0 \\ c_{31} & c_{32} & m_{11}^{\perp} & m_{12}^{\perp} & * & 0 & * & 0 \\ c_{41} & c_{42} & m_{21}^{\perp} & m_{22}^{\perp} & * & 0 & * & 0 \\ 0 & 0 & 0 & 0 & 1 & 0 & 0 & 0 \\ * & * & * & * & * & 1 & 0 & 0 \\ 0 & 0 & 0 & 0 & 0 & 0 & 1 & 0 \\ * & * & * & * & 0 & 0 & * & 1 \end{pmatrix} \begin{pmatrix} \delta\gamma_1^{\parallel} \\ \delta\gamma_2^{\parallel} \\ \delta\gamma_1^{\perp} \\ \delta\gamma_2^{\perp} \\ \delta E \\ \delta\tau \\ \delta L \\ \delta\phi \end{pmatrix} (0)\,, \tag{32}$$

where the asterisks denote nonzero matrix elements which are of no importance for the stability analysis. In the general case of motion outside the symmetry planes the coupling elements c_{ij} are nonvanishing. Then the stability indices of the two local degrees of freedom perpendicular to the PO are obtained by diagonalizing the upper left (4×4) matrix after one period T and eigenvalues of loxodromic form are possible. However, for trajectories located in one of the symmetry planes the c_{ij} are all zero, i.e., the local degrees of freedom decouple to within and perpendicular to the symmetry planes. The 64 equations of motion (23) can be reduced to eight relevant differential equations by integrating the two (2×2) submatrices directly with the help of Eq. (31). The local transformation and the relevant $\boldsymbol{l}$ matrix for the case *(ii)* with $\Theta = \pi$ are specified in Appendix A.

The Lyapunov index λ or the winding number ν (up to multiples of 2π) can be obtained from the traces of the individual (2×2) matrices $(m^{\parallel})_{ij}$ and $(m^{\perp})_{ij}$:

$$\cosh(\lambda) = \tfrac{1}{2}|m_{11} + m_{22}| \quad \text{for} \quad |m_{11} + m_{22}| > 2\,, \tag{33}$$

$$\cos(2\pi\nu) = \tfrac{1}{2}|m_{11} + m_{22}| \quad \text{for} \quad |m_{11} + m_{22}| \le 2\,. \tag{34}$$

Due to the energy scaling property of the Hamiltonian the stability indices are independent of the energy.

The determination of the Morse indices of unstable PO's and the multiples of π for the winding number of stable orbits is essentially given by the number of changes in sign of the m_{12} elements during the propagation of the local monodromy matrix. Details can be found, e.g., in Ref. [25].

IV. THE SYMMETRY PLANE OF THE WANNIER SADDLE

A. General remarks

The symmetry plane of symmetric collective electron motion, where both electron-nucleus distances are identical is known as the Wannier saddle [27]. The electron-pair motion in the phase-space region near the symmetry plane $r_1 = r_2$ plays a dominant role in Wannier's classical description of the three-particle breakup at small energies $E > 0$ [28, 29]. Electron dynamics near the Wannier ridge has also been claimed to be of particular significance for the formation of symmetrically doubly excited resonances below the double ionization threshold [4, 27, 36].

The shape of a potential saddle appears if the three Coulomb potentials of a two-electron atom are considered at fixed hyperradius $\mathcal{R} = \sqrt{r_1^2 + r_2^2}$ as a function of the hyperangle $\alpha = \arctan(r_1/r_2)$ and $\Theta = \angle(\mathbf{r}_1, \mathbf{r}_2)$ [27]. For *fixed* $\mathcal{R}$ the motion on the Wannier ridge $(\alpha = \pi/4)$ is in an unstable equilibrium of the coordinate α. Due to this observation motion along the Wannier ridge is usually regarded to be unstable in general [27]. However, for a quantitative stability analysis the couplings between all the three dynamical variables (r_1, r_2, Θ) [or equivalently $(\mathcal{R}, \alpha, \Theta)$] have to be considered.

We will first study the phase-space structure on the Wannier saddle as a function of the nuclear charge Z for a two-electron atom with infinite nuclear mass. The results change only marginally by taking into account the finite mass of, e.g., the helium nucleus. In Sec. IV C we will focus on periodic motion of the electron pair. We particularly discuss stability properties with respect to variations perpendicular to the symmetry plane $r_1 \equiv r_2$.

B. Phase-space structure of the isoelectronic sequence

Due to the exchange symmetry of the Hamiltonian with respect to r_1 and r_2 a trajectory which initially lies

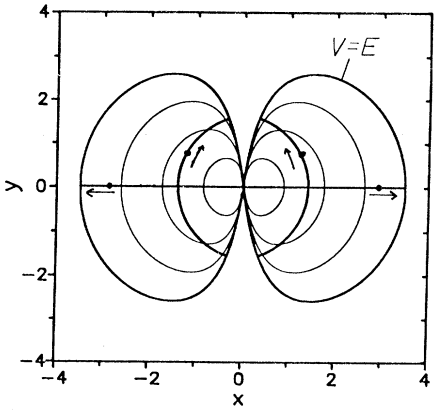

FIG. 1. Equipotential lines and boundary of the classically allowed region on the Wannier saddle ($r_1 = r_2$) with nucleus at $(x, y) = (0, 0)$. ($Z = 2, E = -1$). The Wannier orbit ($y = 0$) and the Langmuir orbit are shown, too.

within the Wannier symmetry plane $r_1 \equiv r_2$, $p_{r_1} \equiv p_{r_2}$ will remain there for all times. The motion on the Wannier saddle is bounded for $Z > 1/4$ and autoionization of an electron is prevented classically. Equipotential lines for this configuration are shown in Fig. 1 as a function of the coordinates

$$x = r\sin(\Theta/2), \quad y = r\cos(\Theta/2), \quad (r = r_1 = r_2)\ . \tag{35}$$

Fundamental PO's are depicted in Fig. 1: The symmetric radial vibration of the electrons with $\Theta \equiv \pi$, i.e., $y = 0$, is the so-called Wannier orbit. The PO of maximum bending vibration (the so-called Langmuir orbit) was orignally studied by Langmuir [30].

The Z dependence of the boundary of the classical allowed region is shown in Fig. 2. For $Z = 1/4$ the energetically accessible configuration space degenerates to a single point. With increasing Z the boundary of configuration space approaches the y axis since the electron repulsion becomes more and more compensated by the nuclear attraction.

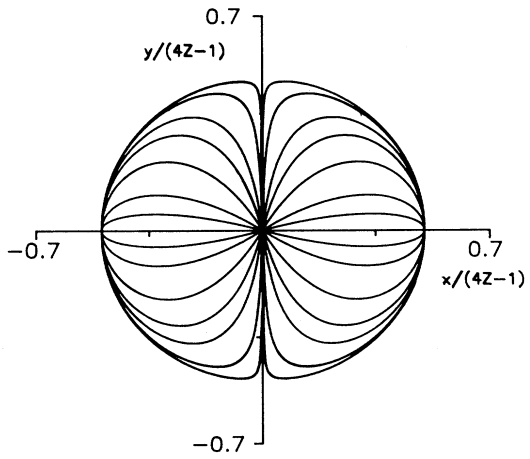

FIG. 2. Boundary of the classical allowed region as a function of Z, $Z = 0.26$, 0.3, 0.5, 1, 2, 10, 100 (from the inner to the outer curve; Z-scaled coordinates used).

It is convenient to visualize the phase-space structure by taking Poincaré surfaces of section (SOS). Such sections are shown in Fig. 3 for different nuclear charges. The phase-space position $X = \pm\sqrt{8\,x/(4\,Z-1)}$ and $P_X = \sqrt{x/(4\,Z-1)}\,p_x$ of the symmetric electron pair is monitored at the surface of section $y = 0$ ($\Theta = \pi$). The use of Z-scaled variables allows a better comparison for systems with arbitrary Z while the regularized momentum P_X gives rise to a compact surface. The symmetric structure of the Poincaré SOS mirrors the symmetric motion of the electrons. The boundary of the SOS corre-

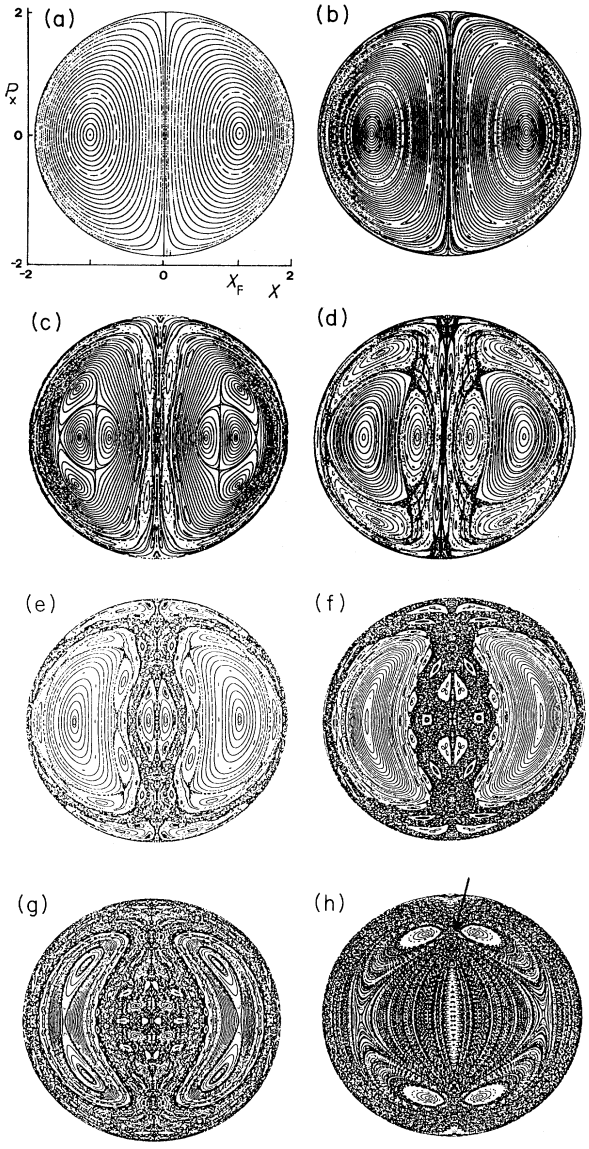

FIG. 3. Poincaré surface of section ($\Theta = \pi$) for symmetric electron configurations. (a) $Z = 0.26$, (b) $Z = 0.43$, (c) $Z = 0.75$, (d) $Z = 1$, (e) $Z = 2$, (f) $Z = 5$, (g) $Z = 10$, (h) $Z = 100$.

sponds to the Wannier orbit itself which lies entirely in the Poincaré SOS.

Figures 3(a)–3(h) illustrate the transition from regular to chaotic motion for increasing nuclear charge Z. The phase space for $Z \approx \frac{1}{4}$ [Fig. 3(a)] exhibits a torus structure with tori grouped around two central fixed points which correspond to the Langmuir orbit (and its symmetry-imaged orbit). The tori indicate the existence of an additional constant of motion in the limit $Z \to 1/4$. The analytical form of this integral of motion — derived in Appendix B — reads

$$I = 2^{\frac{1}{4}} \frac{r-x}{\sqrt{r+x}} \left[1 + \frac{r^2}{16} \frac{r+x}{(r-x)^2} (\dot{r} - \dot{x})^2\right] . \quad (36)$$

Its existence can be related to an adiabatic separation of a (fast) bending and a (slow) radial electronic vibration in the limit $\epsilon = (Z - 1/4) \to 0$. Assuming the adiabatic invariance of I for small ϵ we derive from the value of I on the surface of section $\Theta = \pi(r = x)$ the analytic approximation

$$x_F = \pm \frac{4Z-1}{6} \quad (37)$$

for the position x_F of the central fixed point. Table I shows a comparison between the analytic and the exact numerical results as a function of ϵ.

The small parameter ϵ measures the strength of the perturbation of the integrable system at $Z = 1/4$. As shown in Fig. 3 an increasing number of (resonant) tori is destroyed with increasing perturbation parameter ϵ. New chains of elliptical and hyperbolical fixed points appear and regions of chaotic motion appear and expand with increasing ϵ. Such a behavior is in accordance with the KAM theory [31].

The physically relevant cases $Z = 1$ (H^-) and $Z = 2$ (helium) [Figs. 3(d,e)] exhibit a mixed phase space of regular and chaotic motion. However, the dominant elliptic island around the Langmuir-orbit fixed point remains preserved. This indicates that the constant of motion is approximately conserved for H^- and helium. The bending modes around the Langmuir fixed point are basically more stable than electron-pair motion of dominant radial motion which is located near the Wannier orbit outside the large stability island.

At $Z \approx 5.6$ the Langmuir orbit becomes unstable and bifurcates a pair of stable bending orbits which are no longer symmetric with respect to the x axis.

The limit of large nuclear charge ($Z = 100$) is depicted in Fig. 3(h). Except for the four small elliptical islands (of predominant bending motion) the whole phase space is covered with so-called remnants of tori (Cantori) [32]. The electrons are located on these remnants in the SOS as long as the trajectories do not enter the region near the triple collision $x = 0$ [indicated by an arrow in Fig. 3(h)] where they are "scattered" to another remnant. The independent-particle limit of large Z, $1/Z \to 0$, cannot be handled by means of the KAM theory because the classical motion for $1/Z = 0$ is highly degenerated, i.e., all tori possess resonant frequencies.

C. Periodic motion on the Wannier ridge

1. *Stability with respect to the hyperangle α*

The Poincaré SOS in Fig. 3 provides information on the phase-space structure within the Wannier symmetry plane. However, the stability of trajectories with respect to the hyperangle α outside the symmetry plane cannot be studied in a simple way with the help of surfaces of section. We determine the stability of PO's with respect to α by calculating the monodromy matrix (see Sec. III B). We therefore obtain (in linear approximation) the stability behavior of trajectories near the Wannier saddle.

Our calculations of the stability of the 25 shortest PO's for helium (which appear as fixed points in the SOS) reveal that all PO's are extremely unstable with respect to α except for the Langmuir orbit, which turns out to be stable [33]. On the average, the Lyapunov exponents of the unstable PO's are about ten times larger than those in the collinear symmetry plane to be discussed below (Sec. V). As a consequence, slight deviations from the symmetric configuration outside the symmetry plane lead to rather fast autoionization of one electron.

2. *The Langmuir orbit*

The Langmuir orbit (the shortest PO of the helium atom) turns out to be stable with respect to all degrees of freedom. It is surrounded by an island of stability in phase space, indicating the existence of an additional (local) constant of motion [33]. This shows particularly that the motion of the electron pair in the helium atom is *not* ergodic. The frequently mentioned opinion [34, 35] that the motion on the Wannier ridge is unstable in general is revised, too.

The Langmuir orbit is completely stable only for helium. In all other cases of integer Z the orbit is unstable

TABLE I. Comparison between the approximate analytical [Eq. (37)] and the numerical position of the fixed point x_F corresponding to the Langmuir orbit.

Z	$\epsilon = Z - 1/4$	x_F^{anal}	x_F^{num}
0.2501	0.0001	6.6667×10^{-5}	6.6669×10^{-5}
0.27	0.02	0.01333	0.01339
0.5	0.25	0.167	0.175
1	0.75	0.50	0.56
2	1.75	1.17	1.40

with respect to the hyperangle α [33].

A semiclassical quantization of the Langmuir orbit has been proposed by several authors to approximate the helium ground state [30, 34, 37]. However, the quantization failed due to the use of incorrect quantization conditions, i.e., an incorrect consideration of the motion off the PO. The number of quantum states associated with the torus structure of the stability island around the Langmuir orbit is approximately given by the phase-space volume of the island [38], which scales with the energy as $|E|^{-3/2}$. Nevertheless, the island around the Langmuir orbit is rather small and we expect long-lived resonant states associated with the tori of the island only in the limit of extremely high double excitation [33]. However, in a recent work Müller *et al.* obtained resonance energies with reasonable accuracies for moderately-doubly-excited states via quantization of the torus structure around the Langmuir orbit [16]. They claimed the energetically uppermost states of the intrashell states to be of Langmuir type [17]. On the contrary, quantum calculations for moderately-doubly-excited states for helium (with principal quantum numbers $N < 8$) revealed that those resonances are related to collinear configurations of the type to be discussed in Sec. VI [39].

3. *The Wannier orbit*

A further short symmetric PO is the Wannier orbit with $r_1 \equiv r_2$ and $\Theta \equiv \pi$. It has attracted particular attention since it represents the bounded analogue of the symmetric electron trajectories leading to the classical three-particle breakup for $(E > 0)$. It has been further used to describe the electron dynamics in symmetrically doubly excited states in H^- and helium [4, 27, 40, 41]. A quantitative measure for the quantal significance of this orbit (within the semiclassical framework of the PO theory) is given by a classical stability analysis.

The Wannier orbit is shown in Fig. 4 for $0 < L < L_{\max} = 2(Z - 1/4)$. In the general case of $L \neq 0$ the two electrons move symmetrically on (exact) Kepler ellipses. For $L = L_{\max}$ the two ellipses become identical circles in configuration space with the electrons moving on opposite sides on the circle. For this particular case the stability indices are given analytically by [42]

$$\lambda_\alpha = 2\pi\sqrt{\frac{1}{4Z-1}\left[-(2Z-1)+2\sqrt{Z(Z+2)}\right]}, \tag{38}$$

$$\nu_\Theta = \sqrt{\frac{1}{4Z-1}\left[(2Z-1)+2\sqrt{Z(Z+2)}\right]}\,. \tag{39}$$

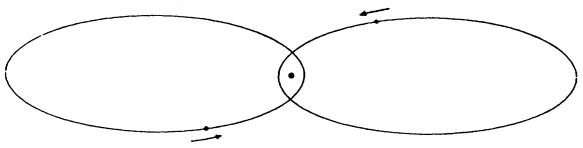

FIG. 4. Schematic view of the Wannier orbit ($\Theta = \pi$, $r_1 = r_2$) for nonvanishing total angular momentum.

λ_α is the Lyapunov exponent with respect to variations in α. The winding number ν_Θ describes (for $L = L_{\max}$) the stability with respect to off-collinear variations in the initial conditions.

For $L \to 0$ the Wannier orbit degenerates to a collinear straight line motion of the electrons (see Fig. 1) including the triple collision with the nucleus. The motion is unstable with respect to the coordinate α for all L and Z and λ_α behaves asymptotically $(L \to 0)$ as

$$\lambda_\alpha \sim -A(Z)\,\ln L\,, \tag{40}$$

with $A(Z) > 0$ varying smoothly with Z. From Eq. (40) we find that λ_α becomes infinite in the limit $L \to 0$. This reflects the nonregularizability of the motion at the triple collision. We obtain the "real" angular momentum L_E at arbitrary energy by rescaling of L, $L_E = L/\sqrt{|E|}$. This shows that for given real angular momentum the scaled angular momentum L always tends to zero if we approach the double ionization threshold $E \to 0$, i.e., $\lambda_\alpha \to \infty$. Due to the diverging Lyapunov exponent we expect no resonant structures in the quantum level density related to the Wannier orbit. This semiclassical prediction has been confirmed now by indepedent quantum calculations which show that wave functions are not localized along the Wannier orbit [11, 14, 39].

V. THE e^-Ze^- CONFIGURATION

Next we will consider the collinear configuration with the electrons located on different sides of the nucleus $(\Theta = \pi)$. This system is of principal interest from a classical point of view as it is conjectured to be purely hyperbolic with a well defined Markov partition of the phase space [9]. Furthermore, a semiclassical PO quantization using only the periodic orbits of the collinear configuration leads to a good approximation for the quantal states localized in the collinear symmetry plane [11].

The main characteristics of the corresponding potential surface (see Fig. 5) are the two ionization channels for $r_1, r_2 \to \infty$ and the symmetry line $r_1 = r_2$ (which is traced by the Wannier orbit described above). The topology of the potential is similar to potential surfaces of triatomic molecules of ABA type below the three-particle breakup [36, 43]. The potential surface has singularites at $r_1, r_2 = 0$, i.e., at the binary collisions of one electron with the nucleus. The binary collisions are regularizable (see Sec. III) and the trajectories can be continued through the singularity using, e.g., the regularized coordinates (9) and the fictive time (10).

The triple collision for which all particle distances vanish plays a key role in understanding the motion of the electron pair. The equations of motion are nonregularizable in this point, i.e., trajectories going into the triple collision cannot be continued uniquely. There exists a one parameter family of orbits starting or ending in the triple collision. They form a purely stable and unstable manifold, the so-called collision manifold [44]. In Fig. 5 a triple collision orbit is shown together with two neighboring trajectories passing close to the triple col-

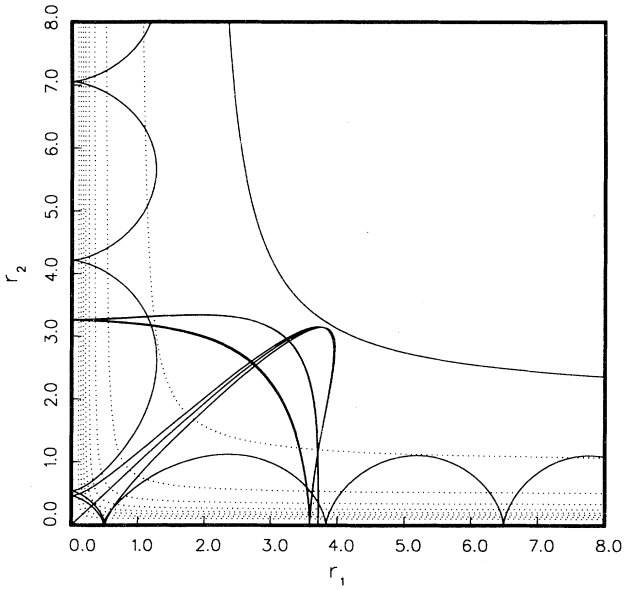

FIG. 5. Equipotential lines (dotted lines) of the collinear configuration e^-Ze^- with $Z = 2$ together with the collision trajectory $(-+)$ and two neighboring ionizing trajectories; r_1, r_2 are the energy-scaled electron-nucleus distances.

lision and subsequently ionizing along the two different channels $r_{1,2} \to \infty$.

We now introduce the motion in the fundamental domain. It is generated by the Hamiltonian with the additional constraint $r_2 < r_1$ induced by an elastically reflecting wall at $r_1 \equiv r_2$. The desymmetrized trajectories in the fundamental domain contain the full information. The procedure corresponds to the classical consideration of the Pauli symmetry principle.

With respect to this reduced phase space, the stable and unstable collision manifold tessalate the phase space and generate a Markov partition. Each time the unstable manifold crosses the Poincaré surface it divides the plane into 2^n distinct cells, where n is the total number of intersections of the manifold with the surface. By reversal of time a similar structure is generated by the stable manifold. Figure 6 shows the first two intersections of the stable manifold with the two-dimensional SOS $r_2 = 0$. Again, we use regularized coordinates $Q_1 = \sqrt{r_1}$, $P_1 = 2\sqrt{r_1}\, p_{r_1}$ to visualize the SOS. The partition of the SOS into cells leads to a symbolic dynamics of the system; every trajectory can be labeled with a binary code according to the rule [9] +, when there is no bounce with the $r_1 \equiv r_2$ boundary wall between two consecutive crossings of the Poincaré surface; −, when there is a bounce. Note that there can be at most one bounce between two crossings of the SOS which guarantees the uniqueness of the coding. The boundaries between the + and − labels are obviously generated by the collision manifolds. The existence of the Markov partition guarantees the completeness of the symbolic dynamics, i.e., every binary code is represented by at least one trajectory. To show the purely hyperbolic behavior of the system it would suffice to prove that the partitioning of phase space gets arbitrarily fine in the limit $n \to \pm\infty$, i.e., that the volume of each Markov cell shrinks to zero. This is confirmed by numerical investigations, but, unfortunately, we do not know of any rigorous proof for this. Indeed, for the positronium negative ion (which differs from the helium atom in that the "nuclear" charge and mass are unity) the shortest PO of the collinear configuration is stable [26] and the corresponding Markov cell remains finite in the limit $n \to \pm\infty$.

For a *generating* Markov partition not only the volume of the cells but also the surfaces of the cells tend to zero. The intersections between the stable and unstable manifolds are then nowhere tangential. Orbits of marginal stability, i.e., with monodromy matrix eigenvalues of unity, are an indicator for tangential intersections of the manifolds. For the collinear configuration such a marginally stable periodic orbit (with code +) exists. It represents an ionized electron 1 with zero kinetic energy at $r_1 = \infty$, while the inner electron 2 moves on a degenerated Kepler ellipse around the nucleus. The existence of this marginally stable orbit causes a cell with a finite surface in the Markov partition even though its volume shrinks to zero for arbitrarily fine partitions.

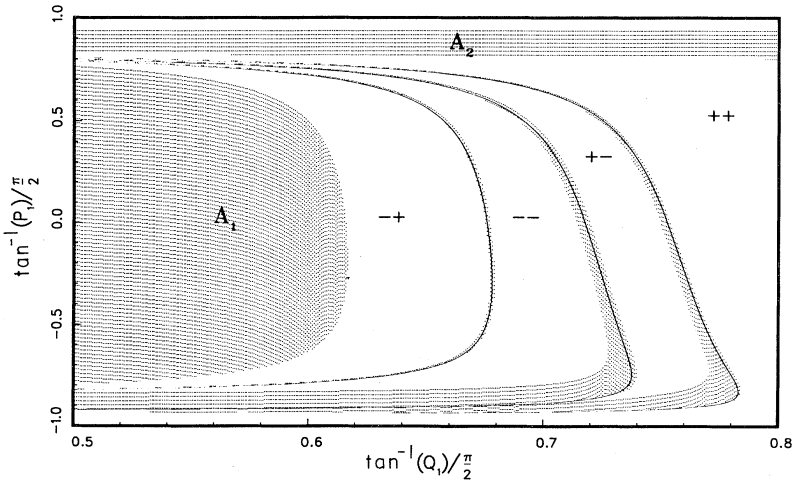

FIG. 6. Markov partition of the Poincaré surface of section $r_2 = 0$ with respect to the regularized coordinates $Q_1 = \sqrt{r_1}$, $P_1 = 2\sqrt{r_1}\, p_1$ for $Z = 2$. The collision manifold (solid line) is surrounded by an ionization region (dotted area); the large areas labeled A_1 and A_2 belong to phase-space points of trajectories which fulfilled the ionization criterion (41) already at the first return to the surface of section.

The collinear e^-Ze^- configuration represents an open system, i.e., one of the electrons can escape with an arbitrary amount of kinetic energy, while the other remains bounded to the nucleus. An ionization boundary cannot be defined in coordinate space since trajectories arbitrarily far away can return to the nucleus. However, one can give an appropriate ionization criterion in phase space which is applicable at the outer turning point of the inner particle 2. If the outer electron 1 has enough kinetic energy to escape in the situation of two static charges, (e.g., $p_1^2/2 - 2/r_1 + 1/r_{12} > 0$), it will certainly ionize in the dynamic case also. This leads to the criterion, that whenever

$$p_2 = 0 \quad \text{and} \quad p_1 > 0, r_2 \leq Z \qquad (E = -1), \qquad (41)$$

the outer electron is ionized and will never return to the nucleus. In Fig. 6 the regions in the SOS $r_2 = 0$ are shown which fulfill the ionization criterion within two intersections with the surface of section. There are two big regions (labeled A_1 and A_2 in Fig. 6) belonging to trajectories which will ionize in a single step without participating in the chaotic dynamics. Most of them belong to the simple reaction $e^- + \mathrm{He}^+ \rightarrow e^- + \mathrm{He}^+$, when an incoming electron scatters without significant time delay in the inner region. This type of ionization occurs also when the electron-electron interaction is switched off.

A different ionization mechanism is related to the stable collision manifold which is surrounded by a layer of ionizing trajectories in the SOS. The boundaries of this layer are generated by the stable manifold of the marginal stable orbit (+) at infinity. By time reversal there exists an equivalent mechanism to capture an electron from $r_1 = \infty$ along the unstable manifold into the chaotic region near the triple-collision point. The existence of this type of ionization (or temporary capture) is related to the existence of the chaotic electron-pair motion and to the nonvanishing interaction between the electrons.

Hence, there are two (dynamically) separated regions in phase space, a chaotic region with strong correlations between the two electrons and an ionization regime with quasi noninteracting electrons. The regions in phase space of both types of ionization processes are connected through the stable and unstable manifolds of the triple collision.

For the calculation of classical quantities such as entropies, escape rates, etc. [23], but also for semiclassical PO quantization [45], the set of all periodic orbits of the system is of particular interest. As the Markov partition is complete, every Markov cell contains a PO characterized by the code of the cell and for every finite binary code there is a PO. We calculated all the PO's up to symbol length 16 (8800 in numbers), all of which are unstable with respect to variations of the collinear radial motion. However, nearly all of them are stable in the bending degree of freedom perpendicular to the symmetry plane. We also found some orbits which are unstable, but the instabilities are always very small compared to those in the symmetry plane.

As already mentioned above, the marginally stable orbit (+) at infinity plays a particular role. The existence of this orbit has influence on certain properties of families

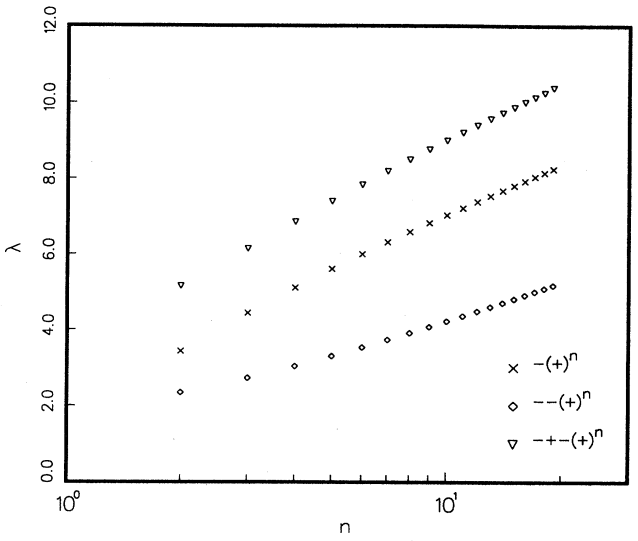

FIG. 7. Lyapunov exponent versus symbol length for the families of periodic orbits $-(+)^n$, $--(+)^n$, and $-+-(+)^n$ ($Z = 2$). The instability $\Lambda = e^\lambda$ for these families grows algebraically (not exponentially) with the symbol length of the orbits.

of PO's containing long (+) sequences in their code. The orbits of these families approach the stable manifold of the marginally stable orbit when increasing the number n of (+) labels. For these orbits the stability exponent λ does not increase linearly with n (or equivalently with the period T) but behaves as

$$\lambda \rightarrow \alpha \ln n \sim \beta \ln T \qquad (42)$$

for $n, T \rightarrow \infty$. This behavior is shown in Fig. 7 for the three shortest families $-(+)^n$, $--(+)^n$, and $-+-(+)^n$, for which we find α values of 1.84, 1.52, and 2.06, respectively. Thus the divergence rate per time λ/T tends to zero in the escape channels $r_{1,2} \rightarrow \infty$ and the motion becomes quasi-integrable for large electron-electron distances. This quasi-integrability corresponds to the adiabatic separation of the fast motion of the inner electron and the slow motion of the outer electron.

VI. THE Ze^-e^- CONFIGURATION

This section deals with the classical motion of the electrons located near the collinear symmetry plane $\Theta = 0$, i.e., both electrons are on the same side of the nucleus. The fundamental periodic motion of such a collinear arrangement is a coherent oscillation of both electrons with the same frequency. The inner electron moves on a slightly perturbed Kepler ellipse with vanishing eccentricity. The outer electron oscillates in an effective dynamical potential well formed by the attractive nuclear force dominant at large distances and the inter-electron repulsion at short distances. The minimal nuclear charge to bind the outer electron in such a configuration is $Z > 1$,

for which the nuclear charge dominates the asymptotic ($r_1 \to \infty$) Coulomb force. The inter-electron repulsion prevents the outer electron from penetrating into the region close to the nucleus. For helium ($Z = 2$) the outer electron stays nearly frozen at some fixed radial distance while the inner electron oscillates between the nucleus and its outer turning point [12, 13].

We investigate the dynamical stability of these collinear configurations by taking Poincaré SOS as depicted in Fig. 8 for helium. The phase-space position $\{r_1, p_1\}$ of the outer electron is monitored each time the inner electron collides with the nucleus ($r_2 = 0$). The fundamental periodic motion described above appears as the elliptic fixed point in the center of an extended torus structure. Near the fixed point the motion of the outer electron is nearly harmonic but for large r_1 the elongated tori reflect an almost Keplerian motion. The open manifolds surrounding the closed tori represent regular trajectories which lead to ionization of the outer electron. If the initial distance is smaller than a critical value, $r_1 \approx 5$ while the inner electron 2 is at the nucleus, the outer electron is "kicked" out of the atom and ionizes immediately.

The fundamental periodic orbit (the fixed point in Fig. 8) is also stable with respect to variations of the initial condition perpendicular to the symmetry plane, i.e., when the electrons move in a (slightly) off-collinear arrangement [13]. Therefore the periodic orbit for $Z = 2$ is embedded in a six-dimensional island of stability in phase space. It is also stable for finite scaled angular momentum $L \neq 0$ as was shown in Ref. [46], where this type of electron motion was "rediscovered" and analyzed (their type-2 configuration).

From Fig. 8 we conclude that the collinear configuration is hardly distinguishable from an integrable system. Consequently, the Hamiltonian can be written to a very good approximation as a function of two action variables J_1, J_2 [10],

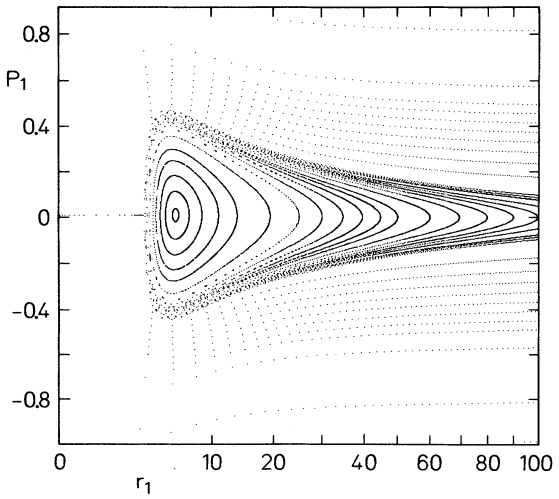

FIG. 8. Poincaré surface of section ($r_2 = 0$) for collinear configurations with both electrons on the same side of the nucleus ($Z = 2$). Scaled phase-space coordinates (r_1, P_1) used.

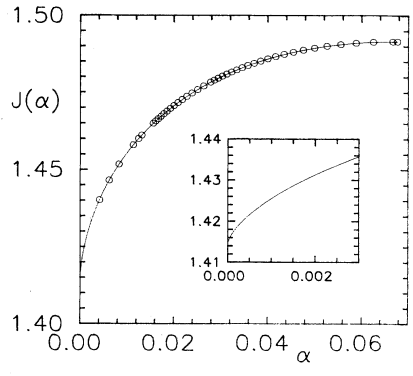

FIG. 9. Accumulated actions of collinear periodic orbits (drawn as circles) after the first return to the SOS as a function of their winding number α. The solid line represents a semianalytical fitting function.

$$H(p_1, r_1, p_2, r_2) = H(J_1, J_2)\,. \tag{43}$$

The action variables measure the symplectic area enclosed by the different independent circuits around the tori.

The main information of the SOS, Fig. 8, is then contained in the energy-surface plot $H(J_1, J_2) = \text{const}$ in the J_1/J_2 action plane. Unfortunately, there is no general procedure to derive the action (and conjugated angle) variables analytically. However, we will now outline how they can be determined numerically [47].

The total action J of a (not necessarily periodic) trajectory accumulated after one closure of the circuit 2 on the torus is given by

$$J(\alpha) = J_2 + \alpha J_1\,, \tag{44}$$

where the winding number α is given by the frequency ratio

$$\frac{\partial H/\partial J_1}{\partial H/\partial J_2} = \frac{\omega_1}{\omega_2} = \alpha \tag{45}$$

of the motion. For the central fixed point of the torus structure in Fig. 8 the winding number can be determined by the linear stability analysis of the corresponding periodic orbit, i.e., $\alpha_{\rm PO}$ is given by the eigenvalues $\exp(\pm 2\pi i\alpha)$ of the orbit's monodromy matrix [Eq. (34)]. For the periodic orbit the dimension of the torus reduces by one and the symplectic area enclosed by the circuit 1 vanishes, i.e.,

$$\left.\frac{dJ}{d\alpha}\right|_{\alpha_{\rm PO}} = J_1 = 0\,, \quad J(\alpha_{\rm PO}) = S_{\rm PO} \tag{46}$$

with $S_{\rm PO} = 1.491\,499$ and $\alpha_{\rm PO} = 0.067\,650$ [13].

For rational $\alpha = r/s$ the orbits close themselves after s revolutions and are again periodic. In the (exactly) integrable case there is a continuously connected family of periodic orbits on the corresponding rational torus. However, even under an infinitesimal perturbation such a resonant torus will generically break up and only two periodic orbits survive (Poincaré-Birkhoff theorem) [10],

one of which is stable and one of which is unstable. With increasing perturbation strength the actions of these two orbits will differ. Their differences are a measure of the strength of the nonintegrable part of the Hamiltonian neglected in (43).

We here use the actions of the periodic orbits with rational winding numbers to approximate the action functional (44). We find that the actions of the stable and unstable orbits differ by less than 10^{-6} which is the accuracy with which we determine the action integrals numerically. In Fig. 9 we plot the actions of 43 different periodic orbits for helium together with a fitting function to be explained below. Obviously, the action functional gets stationary at $\alpha = \alpha_{\rm PO}$ and then decreases monotonically to $J(0) = Z/\sqrt{-2E}$.

To understand the behavior of the action functional as $\alpha \to 0$ it is instructive to investigate the helium atom with the electron-electron interaction approximated by its monopole expansion, which may be justified when the radial distances ($r_1 \gg r_2$) and periods ($\alpha = T_2/T_1 \to 0$) largely differ,

$$H_M = \left(\frac{p_2^2}{2} - \frac{Z}{r_2}\right) + \left(\frac{p_1^2}{2} - \frac{Z-1}{r_1}\right). \tag{47}$$

By simply applying Kepler's laws one derives from (47) the action functional

$$J_M(\alpha) = \frac{Z}{\sqrt{-2E}}\left[1 + \left(\frac{Z-1}{Z}\alpha\right)^{2/3}\right]^{3/2}. \tag{48}$$

The monopole approximation already gives the calculated actions to within an accuracy of 10%. It does not, however, reflect the stationary behavior at $\alpha = \alpha_{\rm PO}$ which is due to higher multipole components in the interelectron potential. The simple ansatz

$$J_M + c_1\alpha + c_2\alpha^2, \tag{49}$$

however, can be used to enforce the conditions (46), which determines c_1 and c_2. This semianalytical formula reproduces the calculated actions to within an average error of 0.1%. Finally, one can approximate the remaining difference by a convenient fit function which preserves the correct boundary conditions as $\alpha \to 0$ and $\alpha \to \alpha_{\rm PO}$. We find that with the choice

$$J(\alpha) = J_M + c_1\alpha + c_2\alpha^2 + J_{\rm diff}(\alpha), \tag{50}$$

where

$$J_{\rm diff} = \sum_{n=3}^{n_{\max}} d_n \alpha^{n/3}(\alpha - \alpha_{\rm PO})^2, \tag{51}$$

it is sufficient to incorporate terms up to $n_{\max} = 5$ to reproduce all the data within an error of less than 10^{-6}. The corresponding function $J(\alpha)$ is drawn as a solid line in Fig. 9.

The action functional can now be used to calculate the individual actions J_1 and J_2,

$$J_1(\alpha) = \frac{dJ}{d\alpha}, \quad J_2(\alpha) = J(\alpha) - \alpha J_1(\alpha), \tag{52}$$

and to plot the energy shell in the J_1/J_2 plane, which is done in Fig. 10. Note that as $J_1 \to 0$, J_2 tends to $S_{\rm PO}$ whereas J_1 becomes singular as J_2 approaches $Z/\sqrt{-2E} = \sqrt{2}$. The singularity reflects the fact that all the energy is stored in the inner electron, whereas the outer electron approaches the ionization threshold with zero kinetic energy but diverging accumulated action. We remark that with the energy surface at hand, it is straightforward to quantize the action integrals separately. This has been done in Ref. [48] and the procedure gives very accurate semiclassical predictions for the energies of a certain class of asymmetrically doubly excited quantum states, i.e., the so-called frozen planet configurations [13]. These states directly correspond to the locally integrable classical motion described above.

With increasing nuclear charge we observe a successive destruction of resonant tori and the onset of chaotic motion within the collinear arrangement. The fundamental PO remains stable up to $Z = 12$ but becomes unstable for larger (integer) values of Z.

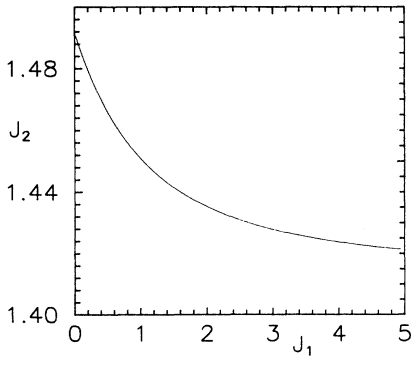

FIG. 10. Energy surface $E = -1$ in the J_1/J_2 action plane for the collinear configuration with both electrons on the same side of the atom ($Z = 2$).

VII. SUMMARY AND CONCLUSION

In the present paper we focus on classical electron-pair motion of two-electron atoms near symmetry planes where the overall motion reduces essentially to two degrees of freedom (for $L = 0$). Consistent with the linear stability analysis in the symmetry plane we approximate the motion of the third (perpendicular) degree of freedom linearly.

Depending on the type of configuration the system shows an amazingly rich structure and a large variety of different types of motion. The collinear configuration with both electrons on the same side is nearly integrable and leads to stable, bounded motion of the electron pair. On the contrary, collinear configurations with the electrons located on different sides of the atom represent a fully hyperbolic system with a Markov partition of the phase space and a binary symbolic dynamics for the periodic orbits of the system. Finally, motion on the Wannier ridge shows a mixed behavior with chaotic and regular motion coexistent. Whereas the structure of the phase

space is rather insensitive to the nuclear charge for the collinear configurations, the phase-space structure on the Wannier saddle depends strongly on Z.

The phase-space regions around the symmetry planes are of particular importance for a semiclassical understanding of the quantum system and allow one to describe a large number of series of doubly excited states (semi)classically. However, a systematic classical analysis of the total six-dimensional phase space remains desirable, even though such an analysis is a hard and still unsolved problem. The problem becomes even harder for total angular momentum $L \neq 0$, where the phase-space dimension increases to eight.

ACKNOWLEDGMENTS

We wish to thank E. Bogomolny, who provided the derivation of the approximate constant of motion for symmetrical electrons given in Appendix B, and G. S. Ezra for collaboration at the early stage of the research. The research was supported by the Deutsche Forschungsgemeinschaft (Grant Nos. Wi877/2 and Wi877/5), and partly by the SFB 276 located in Freiburg.

APPENDIX A: LOCAL COORDINATES FOR THE COLLINEAR CASE $\Theta = \pi$

For the collinear configuration with electrons on opposite sides of the nucleus, i.e., $Q_2 = Q_3 = P_2 = P_3 = 0$, the gradients of H and L

$$\nabla H = (H_{Q_1}, 0, 0, H_{Q_4}, H_{P_1}, 0, 0, H_{P_4})^T, \qquad \nabla L = (0, -P_1, P_4, 0, 0, Q_1, -Q_4, 0)^T, \tag{A1}$$

with $H_{Q_{1,4}} = \frac{\partial H}{\partial Q_{1,4}}$, and $H_{P_{1,4}} = \frac{\partial H}{\partial P_{1,4}}$ are perpendicular to each other in every phase-space point of the symmetry plane. Therefore a transformation onto a local orthogonal coordinate system containing the trivial eigenvectors of the monodromy matrix is given by the matrix

$$\mathbf{0} = \left(\gamma_1^{\parallel}, \gamma_2^{\parallel}, \gamma_1^{\perp}, \gamma_2^{\perp}\gamma_E, \gamma_t, \gamma_L, \gamma_\phi\right) = \begin{pmatrix} -H_{P_4}/R_H & H_{Q_4} & 0 & 0 & H_{Q_1}/R_H & H_{P_1} & 0 & 0 \\ 0 & 0 & -Q_4/R_L & -P_4 & 0 & 0 & -P_1/R_L & Q_1 \\ 0 & 0 & -Q_1/R_L & -P_1 & 0 & 0 & P_4/R_L & -Q_4 \\ H_{P_1}/R_H & -H_{Q_1} & 0 & 0 & H_{Q_4}/R_H & H_{P_4} & 0 & 0 \\ -H_{Q_4}/R_H & -H_{P_4} & 0 & 0 & H_{P_1}/R_H & -H_{Q_1} & 0 & 0 \\ 0 & 0 & -P_4/R_L & -Q_4 & 0 & 0 & Q_1/R_L & P_1 \\ 0 & 0 & P_1/R_L & -Q_1 & 0 & 0 & -Q_4/R_L & -P_4 \\ H_{Q_1}/R_H & H_{P_1} & 0 & 0 & H_{P_4}/R_H & -H_{Q_4} & 0 & 0 \end{pmatrix}, \tag{A2}$$

with $R_H = |\nabla H|^2 = (H_{Q_1}^2 + H_{Q_4}^2 + H_{P_1}^2 + H_{P_4}^2)$ and $R_L = |\nabla L|^2 = (Q_1^2 + Q_4^2 + P_1^2 + P_4^2)$.

The traceless generating matrix $\boldsymbol{l}$ in Eq. (31) has the form

$$\boldsymbol{l} = \begin{pmatrix} l_{11}^{\parallel} & l_{12}^{\parallel} & 0 & 0 & * & 0 & 0 & 0 \\ l_{21}^{\parallel} & l_{22}^{\parallel} & 0 & 0 & * & 0 & 0 & 0 \\ 0 & 0 & l_{11}^{\perp} & l_{12}^{\perp} & 0 & 0 & * & 0 \\ 0 & 0 & l_{21}^{\perp} & l_{22}^{\perp} & 0 & 0 & * & 0 \\ 0 & 0 & 0 & 0 & 0 & 0 & 0 & 0 \\ * & * & 0 & 0 & * & 0 & 0 & 0 \\ 0 & 0 & 0 & 0 & 0 & 0 & 0 & 0 \\ 0 & 0 & * & * & 0 & 0 & * & 0 \end{pmatrix}, \tag{A3}$$

where the relevant matrix elements $l_{ij}^{\parallel}$ and $l_{ij}^{\perp}$ are given by

$$l_{11}^{\parallel} = \frac{1}{R_H}[2H_{Q_1Q_4}(H_{Q_4}H_{P_1} + H_{Q_1}H_{P_4}) + (H_{Q_1}H_{P_1} - H_{Q_4}H_{P_4})(H_{Q_1Q_1} - H_{Q_4Q_4} - H_{P_1P_1} + H_{P_4P_4})],$$

$$l_{12}^{\parallel} = -2H_{Q_1Q_4}(H_{Q_1}H_{Q_4} - H_{P_1}H_{P_4}) + (H_{Q_1}^2 + H_{P_4}^2)(H_{Q_4Q_4} + H_{P_1P_1}) + (H_{Q_4}^2 + H_{P_1}^2)(H_{Q_1Q_1} + H_{P_4P_4}),$$

$$l_{21}^{\parallel} = \frac{1}{R_H^2}[\,2(H_{Q_1P_4} + H_{Q_4P_1})(H_{Q_4}H_{P_1} + H_{Q_1}H_{P_8}) - (H_{P_1}^2 + H_{P_4}^2)(H_{Q_1Q_1} + H_{Q_4Q_4}) - (H_{Q_1}^2 + H_{Q_4}^2)(H_{P_1P_1} + H_{P_4P_4})],$$

$$l_{22}^{\parallel} = -l_{11}^{\parallel}\,, \tag{A4}$$

$$l_{11}^{\perp} = \frac{1}{R}[Q_1 H_{P_1} + Q_4 H_{P_4} - P_1 H_{Q_1} - P_4 H_{P_4} + Q_1 P_1 (H_{Q_3 Q_3} - H_{P_3 P_3}) + Q_4 P_4 (H_{Q_2 Q_2} - H_{P_2 P_2}) + (Q_1 P_4 + Q_4 P_1) H_{Q_2 Q_3}],$$

$$l_{12}^{\perp} = Q_1^2 H_{P_3 P_3} + Q_4^2 H_{P_2 P_2} + P_1^2 H_{Q_3 Q_3} + P_4^2 H_{Q_2 Q_2} + 2 P_1 P_4 H_{Q_2 Q_3} + Q_1 H_{Q_1} + Q_4 H_{Q_4} + P_1 H_{P_1} + P_4 H_{P_4},$$

$$l_{21}^{\perp} = -\frac{1}{R^2}(Q_1^2 H_{Q_3 Q_3} + Q_4^2 H_{Q_2 Q_2} + P_1^2 H_{P_3 P_3} + 2 Q_1 Q_4 H_{Q_2 Q_3} + P_4^2 H_{P_2 P_2} + Q_1 H_{Q_1} + Q_4 H_{Q_4} + P_1 H_{P_1} + P_4 H_{P_4}),$$

$$l_{22}^{\perp} = -l_{11}^{\perp}.$$

Here $H_{Q_i Q_j}$, $H_{P_i P_j}$, $i, j = 1, \ldots, 4$ are the second partial derivatives of H with respect to the coordinates Q_i, P_i.

APPENDIX B: THE CONSTANT OF MOTION FOR NUCLEAR CHARGE $Z = 1/4$

The torus structure of the phase space for symmetrical electron motion $r_1 = r_2$ and nuclear charge $Z \to 1/4$ [see Fig. 3(a)] indicates the existence of an additional constant of motion. The following derivation of the integral of motion has been worked out in collaboration with Bogomolny [49].

It is convenient to introduce semiparabolic coordinates

$$v = 2^{\frac{1}{4}} \sqrt{r + x} \quad , \quad u = 2^{\frac{1}{4}} \sqrt{r - x}, \tag{B1}$$

with $r = r_1 = r_2$ and $x = r \sin(\Theta/2)$. By changing to the fictive time $d\xi = dt/r$ we obtain from Eq. (6) for infinite nuclear mass a regularized Hamiltonian for the symmetrical two-electron atom (derivatives with respect to the new time variable ξ are denoted by primes)

$$h = 4\sqrt{2}\,\epsilon = \frac{1}{2}(u'^2 + v'^2) + u^2 + v^2 + 2\sqrt{2}\,\frac{u^2}{v^2 - u^2}\,. \tag{B2}$$

The parameter $\epsilon = Z - 1/4$ which (up to a constant factor) equals the pseudo energy of the system will serve as a measure of the perturbation of the integrable limit $Z = 1/4$. As a first step we study the scaling behavior of the coordinates in the limit $\epsilon \to 0$ by setting $u := \epsilon^{\mu} \tilde{u}$, $v := \epsilon^{\nu} \tilde{v}$ with exponents μ, ν to be determined.

Since all terms of the Hamiltonian (B2) are positive definite we obtain $u, v \underset{\epsilon \to 0}{\longrightarrow} 0$. The last term of the Hamiltonian (B2) must fulfill simultaneously the conditions

$$2\sqrt{2}\,\frac{u^2}{v^2 - u^2} = o(\epsilon) \tag{B3}$$

and

$$2\sqrt{2}\,\frac{u^2}{v^2 - u^2} \underset{\epsilon \to 0}{\longrightarrow} 2\sqrt{2}\,\frac{u^2}{v^2} = 2\sqrt{2}\,\frac{\tilde{u}}{\tilde{v}}\,\epsilon^{2\mu - 2\nu}\,. \tag{B4}$$

We thus obtain $\mu = 1$, $\nu = 1/2$, i.e.,

$$u = \epsilon\,\tilde{u} \quad , \quad v = \sqrt{\epsilon}\,\tilde{v}\,. \tag{B5}$$

The equations of motion of the Hamiltonian (B2) read

$$0 = u'' + 2u\left(1 + 2\sqrt{2}\,\frac{v^2}{(v^2 - u^2)^2}\right) \underset{\epsilon \to 0}{\simeq} u'' + \frac{4\sqrt{2}}{\epsilon\,\tilde{v}^2}\,u\,, \tag{B6}$$

$$0 = v'' + 2v\left(1 - 2\sqrt{2}\,\frac{u^2}{(v^2 - u^2)^2}\right) \underset{\epsilon \to 0}{\simeq} v'' + 2v\left(1 - 2\sqrt{2}\,\frac{\tilde{u}^2}{\tilde{v}^4}\right)\,. \tag{B7}$$

The solution of Eq. (B6) is

$$u = \sqrt{I}\,\sqrt{v}\,\cos\left(2^{\frac{5}{4}} \int_0^{\xi} \frac{d\xi}{v}\right)\,. \tag{B8}$$

The integration constant $\sqrt{I}$ turns out to be the additional constant of motion, since we obtain from [using Eq. (B8)]

$$\left(2^{\frac{5}{4}}\,\frac{u}{v}\right)^2 + u'^2 = \left(2^{\frac{5}{4}}\sqrt{\frac{I}{v}}\right)^2 \tag{B9}$$

the integral of motion

$$I = \frac{u^2}{v} + \frac{1}{4\sqrt{2}} v u'^2\,. \tag{B10}$$

Expressing (u, v) by (x, r) yields Eq. (36).

[1] C. Marchal, *The Three-Body Problem* (Elsevier, Amsterdam, 1990).

[2] P. Camus, T. F. Gallagher, J. M. Lecomte, P. Pillet, and J. Boulmer, Phys. Rev. Lett. **62**, 2365 (1989).

[3] U. Eichmann, V. Lange, and W. Sandner, Phys. Rev. Lett. **64**, 274 (1990); **68**, 21 (1992).

[4] P. G. Harris, H. C. Bryant, A. H. Mohagheghi, R. A. Reeder, C. Y. Tang, J. B. Donahue, and C. R. Quick, Phys. Rev. A **42**, 6443 (1990).

[5] M. Domke, C. Xue, A. Puschmann, T. Mandel, E. Hud-

son, D. A. Shirley, G. Kaindl, C. H. Greene, H. R. Sadeghpour, and H. Petersen, Phys. Rev. Lett. **66**, 1306 (1991).
[6] I. C. Percival, Proc. R. Soc. London, Ser. A **353**, 289 (1977).
[7] H. Friedrich and D. Wintgen, Phys. Rep. **183**, 37 (1989).
[8] M. S. Child, *Semiclassical Mechanics with Molecular Applications* (Clarendon, Oxford, 1991).
[9] D. Wintgen, K. Richter, and G. Tanner, CHAOS **2**, 19 (1992).
[10] M. C. Gutzwiller, *Chaos in Classical and Quantum Mechanics* (Springer, New York, 1990); J. Math. Phys. **8**, 1979 (1967); **10**, 1004 (1969); **11**, 1791 (1970); **12**, 343 (1971).
[11] G. S. Ezra, K. Richter, G. Tanner, and D. Wintgen, J. Phys. B **24**, L413 (1991).
[12] K. Richter and D. Wintgen, Phys. Rev. Lett. **65**, 1965 (1990); J. Phys. B **24**, L565 (1991).
[13] K. Richter, J. S. Briggs, D. Wintgen, and E. A. Solov'ev, J. Phys. B **25**, 3929 (1992).
[14] J.-H. Kim and G. S. Ezra, in *Proceedings of the Adriatico Conference on Quantum Chaos*, edited H. Cerdeira *et al.* (World Scientific, Singapore, 1991).
[15] R. Blümel and W. P. Reinhardt, in *Directions in Chaos*, Vol. 4, edited by B. L. Hao *et al.* (World Scientific, Hong Kong, 1991).
[16] J. Müller, J. Burgdörfer, and D. W. Noid, Phys. Rev. A **45**, 1471 (1992).
[17] J. Müller and J. Burgdörfer, Phys. Rev. Lett. **70**, 2375 (1993).
[18] P. Gaspard, Phys. Rev. A **48**, 54 (1993).
[19] L. A. Pars, *A Treatise on Analytical Dynamics* (Heinemann, London, 1965).
[20] C. L. Siegel, Ann. Math. **42**, 127 (1941).
[21] P. Kustaanheimo and E. Stiefel, J. Reine Angew. Math. **218**, 204 (1965).
[22] S. J. Aarseth and K. Zare, Celest. Mech. **10**, 185 (1974).
[23] R. Artuso, E. Aurell, and P. Cvitanović, Nonlinearity **3**, 325 (1990); **3**, 361 (1990).
[24] E. T. Whittaker, *Analytical Dynamics* (Cambridge University Press, London, 1927).
[25] B. Eckhardt and D. Wintgen, J. Phys. A **24**, 4335 (1991).
[26] K. Richter, doctoral thesis, Universität Freiburg, 1991 (unpublished).
[27] U. Fano, Phys. Rep. **46**, 97 (1983).
[28] G. Wannier, Phys. Rev. **90**, 817 (1953).
[29] B. Eckhardt, Habilitationsschrift, Universität Marburg, 1991 (unpublished).
[30] I. Langmuir, Phys. Rev. **17**, 339 (1921).
[31] V. I. Arnold, *Mathematical Methods in Classical Mechanics* (Springer, New York, 1979).
[32] R. S. MacKay, J. D. Meiss, and I. C. Percival, Phys. Rev. Lett. **52**, 697 (1984).
[33] K. Richter and D. Wintgen, J. Phys. B **23**, L197 (1990).
[34] G. E. Wesenberg, D. W. Noid, and J. B. Delos, Chem. Phys. Lett. **118**, 72 (1985).
[35] U. Fano and A. R. P. Rau, *Atomic Collisions and Spectra* (Academic Press, London, 1986).
[36] J. M. Rost and J. S. Briggs, J. Phys. B **24**, 4293 (1991).
[37] M. S. Dimitrijević and P. V. Grujić, Z. Naturforsch, Teil A **39**, 930 (1984).
[38] M. V. Berry, in *Chaotic Behaviour of Deterministic Systems*, edited by G. Iooss *et al.* (North-Holland, Amsterdam, 1983), p. 172.
[39] K. Richter and D. Wintgen, J. Phys. B (to be published).
[40] W. H. Miller, J. Chem. Phys. **56**, 38 (1972).
[41] H. R. Sadeghpour, Phys. Rev. A **43**, 5821 (1991).
[42] M. Poirier, Phys. Rev. A **40**, 3498 (1989).
[43] R. Schinke and V. Engel, J. Chem. Phys. **93**, 3252 (1990).
[44] R. McGehee, Inventiones Math. **27**, 191 (1974).
[45] P. Cvitanović and B. Eckhardt, Phys. Rev. Lett. **62**, 823 (1989).
[46] T. Yamamoto and K. Kaneko, Phys. Rev. Lett. **70**, 1928 (1993).
[47] O. Bohigas, S. Tomsovic, and D. Ullmo, Phys. Rep. **223**, 45 (1993).
[48] K. Richter and D. Wintgen, Comm. At. Mol. Phys. (to be published).
[49] E. Bogomolny (private communication).